# Structure and Mechanism of ArnA: Conformational Change Implies Ordered Dehydrogenase Mechanism in Key Enzyme for Polymyxin Resistance

**ARTICLE** *in* STRUCTURE · JULY 2005

Impact Factor: 5.62 · DOI: 10.1016/j.str.2005.03.018 · Source: PubMed



**3 AUTHORS**, INCLUDING:

Petia Gatzeva-Topalova
PGT Medical and Scientific Writing
**6** PUBLICATIONS **251** CITATIONS
SEE PROFILE

Marcelo Carlos Sousa
University of Colorado Boulder
**42** PUBLICATIONS **1,792** CITATIONS
SEE PROFILE

Published in final edited form as:
*Structure*. 2005 June ; 13(6): 929–942. doi:10.1016/j.str.2005.03.018.

# Structure and Mechanism of ArnA: Conformational Change Implies Ordered Dehydrogenase Mechanism in Key Enzyme for Polymyxin Resistance

**Petia Z. Gatzeva-Topalova**[1], **Andrew P. May**[2], and **Marcelo C. Sousa**[1,*]

[1]Department of Chemistry and Biochemistry, University of Colorado at Boulder, Boulder, Colorado 80309

[2]Fluidigm Corporation, 7100 Shoreline Court, South San Francisco, California 94080

## Summary

The modification of lipid A with 4-amino-4-deoxy-L-arabinose (Ara4N) allows gram-negative bacteria to resist the antimicrobial activity of cationic antimicrobial peptides and antibiotics such as polymyxin. ArnA is the first enzyme specific to the lipid A-Ara4N pathway. It contains two functionally and physically separable domains: a dehydrogenase domain (ArnA_DH) catalyzing the $NAD^+$-dependent oxidative decarboxylation of UDP-Glucuronic acid (UDP-GlcA), and a transformylase domain that formylates UDP-Ara4N. Here, we describe the crystal structure of the full-length bifunctional ArnA with UDP-GlcA and ATP bound to the dehydrogenase domain. Binding of UDP-GlcA triggers a 17 Å conformational change in ArnA_DH that opens the $NAD^+$ binding site while trapping UDP-GlcA. We propose an ordered mechanism of substrate binding and product release. Mutation of residues $R_{619}$ and $S_{433}$ demonstrates their importance in catalysis and suggests that $R_{619}$ functions as a general acid in catalysis. The proposed mechanism for ArnA_DH has important implications for the design of selective inhibitors.

## Introduction

The main component of the outer membrane of gram-negative bacteria is lipopolysaccharide (LPS). Lipid A is the conserved, bioactive element of LPS and is commonly used as a recognition element for host immune response to infection. As a means of evading the host immune system, bacteria have evolved mechanisms to modify LPS structure in response to environmental stimuli (Gunn, 2001; Gunn et al., 2000a; Guo et al., 1997). One such modification is the addition of 4-amino-4-deoxy-L-arabinose (Ara4N) to phosphate groups in lipid A. This modification can be triggered in *E. coli* and *Salmonella typhimurium* by growth in the presence of vanadate or low concentrations of magnesium (Gunn, 2001; Gunn and Miller, 1996; Gunn et al., 2000b; Guo et al., 1997). The modification of lipid A with Ara4N is responsible for bacterial resistance to the action of cationic antimicrobial peptides



*Correspondence: marcelo.sousa@colorado.edu.

**Supplemental Data**

Supplemental Data including a movie highlighting the conformational changes occurring in ArnA_DH upon substrate binding are available at http://www.structure.org/cgi/content/full/13/6/929/DC1.

**Accession Numbers**

The coordinates and structure factors for all of the structures presented in this manuscript have been deposited in the Protein Data Bank under the following accession numbers: ArnA full-length: 1Z7E; ArnA_DH domain mutants: R619E, 1Z7B; R619M, 1Z75; R619Y, 1Z74; and S433A, 1Z73.

(CAMPs) of the innate immune system and antibiotics like polymyxin (Roland et al., 1993, 1994; Shafer et al., 1984).

CAMPs are small, amphipathic, cationic peptides that interact with the negative charges of the phosphate groups in LPS (Hoffmann et al., 1999; Scott and Hancock, 2000; Zasloff, 2002). These peptides exert their bactericidal action by permeabilizing the bacterial membrane (Matsuzaki, 1999; Shai, 1999; Yang et al., 2000). The addition of Ara4N to a phosphate group in lipid A neutralizes a negative charge on the phosphate and adds a sugar with a positively charged primary amine. This results in a lowered affinity of CAMPs for the modified bacterial membrane that is thought to mediate the resistance mechanism (Peschel, 2002). The modification of lipid A with Ara4N may be responsible, at least in part, for the persistent infections with *Pseudomonas aeruginosa* observed in cystic fibrosis (CF) patients (Peschel, 2002). Membranes of *P. aeruginosa* isolated from CF patients were shown to have the Ara4N modification (Ernst et al., 1999).

The enzymes responsible for the synthesis of Ara4N precursors and its transfer to lipid A are encoded in the *pmrHFIJKLM* operon and the *pmrE* gene (*pmr* = Polymyxin resistance) (Gunn et al., 1998). These proteins are highly conserved in gram-negative bacteria such as *E. coli* and the human pathogens *Pseudomonas aeruginosa*, *Burkolderia cepacia*, *Yersinia pestis*, and all types of *Salmonella* (Breazeale et al., 2005). Nonpolar mutations of the individual proteins in the operon showed that all proteins, except pmrM, are essential for the addition of Ara4N to lipid A and polymyxin resistance (Gunn et al., 2000b), making them excellent potential targets for drug design. Based on sequence similarity to known enzymes, a pathway leading to the synthesis of lipid A-Ara4N has been proposed (Figure 1) (Baker et al., 1999; Breazeale et al., 2002, 2003, 2005; Zhou et al., 1999). Conversion of UDP-Glucose into UDP-Glucuronic acid (UDP-GlcA) is catalyzed by the product of the *pmrE* gene, a well-characterized dehydrogenase (Campbell et al., 2000; Ge et al., 2004; Perozich et al., 1995; Roman et al., 2003; Schiller et al., 1976). ArnA, the first pathway-specific enzyme, is a bifunctional protein whose C-terminal domain catalyzes the $NAD^+$-dependent oxidative decarboxylation of UDP-GlcA to UDP-β-(L-*threo*pentapyranosyl-4″-ulose) (UDP-4-keto-pentose) (Gatzeva-Topalova et al., 2004). The transamination of this intermediate to yield UDP-β-(4-deoxy-4-amino-arabinoase) (UDP-Ara4N) is catalyzed by ArnB in a reaction with a $K_{eq}$ of ~0.1, a value not favoring transamination (Breazeale et al., 2003; Noland et al., 2002). The *N10*-formyltetrahydrofolate-dependent formylation of UDP-Ara4N to produce UDP-β-(4-deoxy-4-formamido-L-arabinose) (UDP-Ara4FN) is catalyzed by the N-terminal domain of the bifunctional ArnA (Breazeale et al., 2005; Gatzeva-Topalova et al., 2005). However, no formylated sugars are observed attached to lipid A. The formylation is thus thought to be a transient step required to compensate for the unfavorable equilibrium of the transamination reaction (Breazeale et al., 2005). The formylated intermediate is then transferred to a membrane bound undecaprenyl-phosphate carrier by ArnC (Breazeale et al., 2005). Raetz and coworkers have recently shown that the ArnC transferase is specific for UDP-Ara4FN in vitro (Breazeale et al., 2005). Additional enzymes in the *pmrHFIJKLM* operon have been proposed to deformylate undecaprenyl-P-Ara4FN and complete the transfer of Ara4N to lipid A. However, their activity has not yet been demonstrated in vitro (Breazeale et al., 2005; Gatzeva-Topalova et al., 2005).

Both the transformylase and dehydrogenase activities catalyzed by ArnA are required for lipid A modification with Ara4N and polymyxin resistance (Breazeale et al., 2005). These activities can be physically separated by expressing the individual ArnA domains (Breazeale et al., 2005; Gatzeva-Topalova et al., 2004, 2005). The N-terminal 300 amino acids encode the transformylase activity, whereas the C-terminal 360 amino acids are responsible for the dehydrogenase activity (we previously referred to this domain as ArnA decarboxylase but hereby adopt the more standard name of ArnA dehydrogenase used by Raetz [Breazeale et

al., 2005; Gatzeva-Topalova et al., 2004]). We have recently solved the crystal structures of each separate domain in the absence of ligands (Gatzeva-Topalova et al., 2004, 2005). The ArnA transformylase domain (ArnA_TF) showed similarity to other *N10*-formyltetrahydrofolate binding enzymes such as glycinamide ribonucleotide formyltransferase (GARF), methionyl-tRNA formyltransferase (FMT), and the N-terminal hydrolase domain of N10-formyl-tetrahydrofolate dehydrogenase ($N_t$-FDH). Mutagenesis data showed that ArnA_TF utilizes a GARF-like mechanism of formyl transfer relying on residues $N_{102}$, $H_{104}$, and $D_{140}$ to catalyze the reaction (Gatzeva-Topalove et al., 2005). The ligand-free structure of the ArnA dehydrogenase domain (ArnA_DH) confirmed the enzyme as a member of the short-chain dehydrogenase/reductase (SDR) family (Gatzeva-Topalova et al., 2004). Comparison with other SDR enzymes allowed modeling of substrate binding to ArnA_DH and suggested that the $NAD^+$ binding site was closed in the ligand-free structure. We thus proposed that a conformational change triggered by UDP-GlcA binding would open the $NAD^+$ binding site. A role for residues $S_{433}$ and $R_{619}$ in catalysis was also suggested based on the substrate binding model and the conservation of these residues in ArnA_DH and other SDR enzymes catalyzing UDP-GlcA decarboxylation (Gatzeva-Topalova et al., 2004).

In this study, we have determined the first structure of full-length ArnA with the natural substrate UDP-GlcA and the $NAD^+$ analog ATP bound to the dehydrogenase domain. A 17 Å conformational change that opens the $NAD^+$ binding site is observed, as predicted from the ligand-free ArnA_DH structure. Unexpectedly, this structural transition also traps UDP-GlcA in its binding site. We propose an ordered mechanism of substrate binding and product release and probe the roles of residues $S_{433}$ and $R_{619}$ in UDP-GlcA decarboxylation by mutagenesis and structural analysis. The implication of this mechanism for the design of selective inhibitors of ArnA is discussed.

## Results

### ArnA Structure Determination and Overall Architecture

The oligomeric state of ArnA in solution was determined by subjecting the purified protein to size-exclusion chromatography followed by multiangle light-scattering analysis. The results showed that ArnA is a hexamer in solution with no sign of lower-order oligomers in the purified preparation (data not shown). Furthermore, the oligomeric state of the full-length protein was independent of the presence of substrates. When expressed separately, the individual transformylase and dehydrogenase domains of ArnA do not form hexamers (Gatzeva-Topalova et al., 2004, 2005). The full-length protein is thus required for hexamerization.

Crystallization of ArnA in the presence of UDP-GlcA and ATP yielded two different crystal forms from the same crystallization conditions. One form diffracted to 3.7 Å resolution, and the crystals belonged to rhombohedral space group R3, with two protomers per asymmetric unit. The second form crystallized in orthorhombic space group $P2_12_12_1$, with six protomers per asymmetric unit and showed diffraction to 3 Å resolution. We were also able to obtain the rhombohedral crystal form with the selenomethionine-labeled ArnA (SeMet). The structure of ArnA was solved by molecular replacement by using the structures of the ligand-free ArnA transformylase domain (PBD ID: 1YRW [Gatzeva-Topalova et al., 2005]) and the ligand-free ArnA dehydrogenase domain (PDB ID: 1U9J [Gatzeva-Topalova et al., 2004]) refined to 1.7 and 2.4 Å resolution, respectively, as search models. The search models represented approximately one-twelfth of the scattering mass in the asymmetric unit of the orthorhombic crystals. Therefore, we first determined the position of the two ArnA protomers in the SeMet rhombohedral crystals by molecular replacement, where the search models represented approximately one-fourth of the asymmetric unit scattering mass. An

anomalous difference Fourier map showed positive peaks (with intensities of 3.5 σ or higher) within 2.0 Å of the selenium atoms for 15 out of the 18 Se-methionines in the models confirming the molecular replacement solutions (the three remaining methionines, M11 in one protomer and M11 and M220 in the other protomer, had positive anomalous peaks at 2.27 Å, 2.9 Å, and 3.7 Å from the selenium atom, respectively). The hexameric biological unit was generated by applying crystallographic symmetry operations in the R3 crystals. This hexamer was then used to solve the structure of the orthorhombic crystals, which contained one hexamer per asymmetric unit. The final model is well refined to 3.0 Å resolution ($R_{work}$ = 0.225, $R_{free}$ = 0.247) with good stereochemistry and 100% of residues lying in the allowed regions of the Ramachandran plot. Data collection and refinement statistics are summarized in Table 1.

Both domains of ArnA are generally well defined in the structure. A short loop in the transformylase domain (residues 35–42), and the interdomain linker comprising residues 305–313 could not be traced unambiguously, presumably due to conformational flexibility (chain D in the coordinate file shows the most complete interdomain linker, missing only residues 309–312).

The hexamer adopts the shape of a three-blade propeller with overall dimensions of 162 × 87 Å (Figure 2). The C-terminal, dehydrogenase domains form the central core of the particle (light green in Figure 2A), while the N-terminal, transformylase domains are arranged on the periphery (dark green in Figure 2A). The dehydrogenase domains in the central core mediate most of the contacts between protomers within the hexamer, which can be considered as a dimer of trimers. The intersubunit contacts in the trimer are dominated by hydrogen bonding and ionic interactions. These include Lys381 and Lys382 from one protomer, which form salt bridges with Asp368 and Glu366, respectively, from a neighboring protomer, as well as Glu374, which hydrogen bonds to the main chain amino groups of Ser373 and Glu374 from a second protomer.

The dimerization interface is an extended hydrophobic surface and includes the formation of a two-stranded antiparallel β sheet (residues 448–456 from two adjacent protomers) and a four-helix bundle (residues 401–423 and 460–480) between two adjacent protomers. The peripheral transformylase domains contribute a few interactions to stabilize the hexamer, but they are limited compared to those from the dehydrogenase domain. The total buried surface in the hexamer is 22,122 $Å^2$.

As shown in Figure 2C (colored by B factor), the dehydrogenase domains in the central core of the particle are more ordered (with a $B_{ave}$ = 32.2 $Å^2$) than the transformylase domains in the outer edges ($B_{ave}$ = 60.8 $Å^2$). During refinement of the structure, the presence of ATP and UDP-GlcA bound to the dehydrogenase domains became evident and were added to the model (Figure 2D). Well-defined electron density is observed for the ligands in the final model (Figure 3). The conformations of the individual domains from all six protomers are essentially identical, superimposing with an average rms deviation of 0.18 Å for the transformylase domains, and 0.33 Å for the dehydrogenase domains for all Cα atoms. While NCS restraints were used throughout the refinement process (see the Experimental Procedures), the weight of those restrains was reduced to 40 Kcal $mol^{-1}$ $A^{-2}$ for the transformylase domain and 80 Kcal $mol^{-1}$ $A^{-2}$ for the dehydrogenase domain in the final rounds of refinement. In addition, inspection of the electron density in a simulated annealing composite omit map did not reveal deviations of any of the protomers from the electron density. We therefore consider all protomers conformationally equivalent and focus our further analysis on the features of the individual domains of a single protomer.

The conformation of the transformylase domain is very similar in the full-length structure presented here and in that of the isolated domain (Gatzeva-Topalova et al., 2005). The two structures superimpose with an rms deviation of 0.66 Å. In contrast, the structure of the ligand-free dehydrogenase domain shows striking differences from the ligand bound structure observed in the full-length hexamer (see below).

## Conformational Changes in the ArnA Dehydrogenase Domain

A comparison of the structures of the ArnA dehydrogenase domain in the presence and absence of ligands reveals a striking conformational change (Figure 4). In the previously determined ligand-free structure, residues 500–509 define a loop that blocks the $NAD^+$ binding site. In contrast, in the presence of UDP-GlcA and the $NAD^+$ analog ATP, this segment of polypeptide forms a short helix that folds over the UDP-GlcA (L1 in Figure 4B). The Cα atom of residue $I_{506}$ in the center of this loop is displaced by 17.5 Å between the two structures, illustrating the magnitude of the conformational change. It is important to note that this region of the structure is not involved in any interactions with the transformylase domain, nor is it involved in any lattice contacts in this ligand bound structure or in the previously determined ligand-free structure. The conformational change thus appears to be induced by ligand binding and has two important consequences: (i) it opens the $NAD^+$ binding site (which in our structure is occupied by ATP) (Figures 4A and 4C); and (ii) it effectively traps the UDP-GlcA in its binding site (Figures 4B and 4D).

Another important conformational change occurs in the region defined by amino acids 605–616. In the ligand-free structure, electron density for this segment of the polypeptide was ill defined and could not be modeled, suggesting conformational flexibility. Upon binding of UDP-GlcA, $S_{606}$–$Y_{609}$ become ordered into a one-turn helix followed by a loop that makes several contacts with the uracil ring of UDP-GlcA (L2 in Figure 4). This conformational change also contributes to the trapping of UDP-GlcA in its binding site. Like in the case of the 500–509 loop, this region is not involved in any interdomain or crystal contacts. Therefore, it appears to be triggered by UDP-GlcA binding.

Several smaller conformational changes are also observed in the ligand bound structure of ArnA. They can be visualized, from a more global perspective, as a small hinge motion between the two dehydrogenase subdomains such that the protein closes in around the substrates to form a more compact structure (see Movie S1 in the Supplemental Data available with this article online).

## Substrate Binding Sites in ArnA Dehydrogenase Domain

The crystal structure of ArnA presented here was determined in the presence of the dehydrogenase substrate UDP-GlcA and ATP. The second dehydrogenase substrate $NAD^+$ contains an ADP moiety, and ATP can act as a close structural mimic of $NAD^+$ as a result. Very clear density for both ligands was observed in the dehydrogenase domain of ArnA (Figure 3).

The dehydrogenase active site is situated in a cleft formed between the two subdomains of ArnA_DH (Figure 2D). The binding site for $NAD^+$ (occupied by ATP in our structure) is located mainly in the N-terminal (Rossmann fold) subdomain of ArnA_DH, as observed in many other dinucleotide binding proteins (Figure 2D). As shown in Figure 5A, the adenosine moiety resides in a hydrophobic pocket formed by residues $L_{321}$, $L_{346}$, $I_{348}$, $I_{369}$, $V_{390}$, $I_{392}$, and $L_{408}$. It also forms hydrogen bonds with the side chain of $D_{368}$ and the main chain nitrogen of $I_{369}$. The ribose and phosphate groups are stabilized by additional hydrogen bonding interactions with the side chain oxygen of $D_{347}$, and the main chain amides of $G_{325}$, $F_{326}$, and $I_{327}$.

The UDP-GlcA binding site resides mainly in the C-terminal subdomain of ArnA_DH, where it makes a number of hydrogen bonding contacts with the protein (Figures 2D and 5B). The uracil moiety hydrogen bonds the main chain atoms of $K_{256}$ and $I_{528}$. The ribose conformation is stabilized by hydrogen bonding the side chains of $Q_{533}$ and $Y_{613}$, while the α and β phosphates are fixed in place by several hydrogen bonds to $R_{460}$, $R_{535}$, and the catalytic $R_{619}$ (see below). The protein also makes seven hydrogen bonds with the glucuronic acid moiety, presumably positioning it in the right conformation for catalysis. The 2″ hydroxyl of the GlcA contacts $Y_{398}$, while the 4″ hydroxyl is within hydrogen bonding distance of $O^{\gamma}{}_1$ of $T_{432}$, a conserved residue in SDR enzymes that catalyze $NAD^+$-dependent oxidation of the 4″ hydroxyl. The carboxyl group of UDP-GlcA that leaves as carbon dioxide during catalysis displays hydrogen bond interactions with the backbone nitrogen of $N_{492}$ as well as with the side chains of $S_{433}$ and $R_{619}$. These two residues were previously suggested to play a role in substrate binding and/or catalysis (Gatzeva-Topalova et al., 2004).

## Role of $S_{433}$ and $R_{619}$ in the Oxidative Decarboxylation Reaction Catalyzed by ArnA Dehydrogenase

We have previously proposed that $S_{433}$ and $R_{619}$ may play a role in the decarboxylation reaction catalyzed by ArnA dehydrogenase (Gatzeva-Topalova et al., 2004). This proposal was based on the strict conservation of these residues in all enzymes catalyzing UDP-GlcA decarboxylation and the fact that residues at equivalent positions in other SDR enzymes have been shown to play important roles in substrate binding and catalysis. In addition, modeling studies suggested that $S_{433}$ and $R_{619}$ would be well positioned to interact with the UDP-GlcA carboxylate (Gatzeva-Topalova et al., 2004). Indeed, the ATP/UDP-GlcA ligand bound structure of the ArnA dehydrogenase domain shows $S_{433}$ to be 2.8 Å and $R_{619}$ to be 3.5 Å from the UDP-GlcA carboxylate.

The potential role of $S_{433}$ and $R_{619}$ in the decarboxylation reaction was investigated by preparing a series of point mutants (S433A, S433T, R619M, R619Y, and R619E) of the isolated ArnA_DH domain (amino acids 306–660). The activity of the mutants was compared to the wild-type ArnA_DH domain by using a spectrophotometric assay under conditions that are saturating for the wild-type enzyme (see legend in Table 2). The results, summarized in Table 2, show that all mutants had undetectable or dramatically reduced activity, supporting a role for these residues in substrate binding and/or catalysis. While the R619Y and R619E mutants had no activity, S433A and R619M showed residual activities 30- and 800-fold lower than the wild-type, respectively. Surprisingly, The S433T mutant had no detectable activity. The S433A and R619M mutants were also evaluated at UDP-GlcA concentrations 5-fold higher than the standard assay. This condition represents a substrate concentration more than 90-fold the apparent $K_m$ for UDP-GlcA in the wild-type enzyme. As shown in Table 2, the 5-fold increase in substrate concentration resulted in a modest 2-fold increase in the activity of the R619M mutant and had no effect on the activity of the S433A mutant. These results suggest that, while $S_{433}$ and $R_{619}$ may play a role in substrate binding and contribute to the affinity of the enzyme for UDP-GlcA, the dramatic loss of activity is likely due to their role in catalysis.

To rule out enzyme misfolding as a factor in the lack of activity in our mutants, crystallization experiments were set up for all the mutant proteins under conditions that had previously resulted in successful crystallization of the isolated wild-type ArnA_DH domain (Gatzeva-Topalova et al., 2004). In spite of repeated efforts, the S433T mutant failed to crystallize, suggesting that the lack of activity in this mutant may be due to improper folding. By contrast, crystals were immediately obtained for the rest of the mutants, and their structures were solved and refined by using difference Fourier methods as detailed in the Experimental Procedures. A superposition of the mutant structures with the wild-type

shows no significant conformational changes due to the substitutions. The mutant structures superimpose with the wild-type ArnA_DH fragment with rms deviations between 0.1 and 0.25 Å for all Cα atoms. In the region of the structure in which the mutations are located (amino acids 432–434 and 619–621), they superimpose with an average rms deviation of 0.21 Å. We therefore conclude that the loss of activity in the mutants (except S433T) is a bona fide effect of the role of $S_{433}$ and $R_{619}$ in enzyme catalysis.

## Discussion

ArnA is a required enzyme in the pathway for the modification of lipid A with Ara4N that leads to antimicrobial resistance in gram-negative bacteria (Breazeale et al., 2005). ArnA is bifunctional. It catalyzes the oxidative decarboxylation of UDP-GlcA with its C-terminal dehydrogenase domain (the first pathway-specific reaction). Formyl transfer from N10-formyltetrahydrofolate to UDP-Ar4N is catalyzed by the N-terminal transformylase domain of ArnA (Breazeale et al., 2005; Gatzeva-Topalova et al., 2005). ArnB, a separate enzyme, catalyzes the intervening transamination reaction (Figure 1). The biochemical and structural data presented here show that ArnA forms a hexameric structure comprising a dimer of trimers. The dehydrogenase domains are arranged at the center of the particle, with the transformylase domains on the outer edges (Figure 2A). Little interaction is observed between the two domains, and the oligomerization does not appear to introduce structural changes that would affect the activity of the individual domains. This is illustrated by the high degree of structural similarity between the transformylase domain in the hexamer with that of the isolated domain (rms deviation of 0.66 Å for 97% of the Cα atoms). It is also in agreement with the observation that the dehydrogenase activity of the full-length hexameric enzyme is indistinguishable from that of the isolated dehydrogenase domain (Gatzeva-Topalova et al., 2004).

Since ArnA catalyzes the first and third steps in the lipid A-Ara4N biosynthetic pathway while ArnB catalyzes the second step (Figure 1), it is tempting to speculate that these enzymes may form a multienzyme complex in which substrates could be channeled (Breazeale et al., 2005;Gatzeva-Topalova et al., 2005). However, no data are yet available supporting the existence of such a complex. It is also possible that additional enzymes in the pathway may be needed for assembly of this complex. It is tempting to speculate that the hexameric structure of full-length ArnA may act as a scaffold for a complex. Further work characterizing the biochemistry and interactions of enzymes within this pathway is required to explore this intriguing possibility.

### Conformational Changes upon Substrate Binding

The comparison of the ligand-free structure of the ArnA_DH domain with the ligand bound structure presented here highlights a striking conformational change (Figure 4). In the ligand-free structure, the binding site for UDP-GlcA is open, while a loop defined by amino acids 500–509 occupies the $NAD^+$ binding site. This observation led to the proposal that UDP-GlcA would bind the enzyme first, inducing a conformational change that would open the $NAD^+$ binding site (Gatzeva-Topalova et al., 2004). The ligand bound structure presented here shows a 17 Å displacement of the 500–509 loop, effectively opening the $NAD^+$ binding site, and provides strong support for the above-described hypothesis. In the ligand bound structure, the $NAD^+$ site is occupied by ATP (an $NAD^+$ analog). Interestingly, the ligand bound structure also highlights an unpredicted consequence of the conformational change. The new conformation of the 500–509 polypeptide and the ordering of the 605–616 region effectively trap UDP-GlcA in the active site (Figures 4B and 4D). This observation might help rationalize the differences between ArnA dehydrogenase and a family of related eukaryotic enzymes that also catalyze UDP-GlcA decarboxylation.

The oxidative decarboxylation of UDP-GlcA is catalyzed in many eukaryotes, including humans, by enzymes alternatively known as UDP-GlcA decarboxylases or UDP-Xylose synthases (Bar-Peled et al., 2001; Harper and Bar-Peled, 2002; Moriarity et al., 2002; Pattathil et al., 2005). These enzymes use $NAD^+$ to oxidize the 4″ hydroxyl of UDP-GlcA, followed by decarboxylation, just as in ArnA. However, in UDP-Xylose synthases, the decarboxylated 4-keto sugar is then rereduced by NADH to generate UDP-Xylose (Figure 6B). Therefore, $NAD^+$ is utilized as a coenzyme and does not need to be added exogenously for the reaction to proceed (Bar-Peled et al., 2001). In contrast, ArnA uses $NAD^+$ as a true substrate that is consumed to release NADH and the decarboxylated UDP-4-keto-pentose (Figure 6A) (Gatzeva-Topalova et al., 2004). The fact that UDP-GlcA appears trapped in the active site of ArnA, while the $NAD^+$ binding site remains open, suggests that, after the oxidation reaction takes place, NADH could be released from the enzyme. This implies an ordered reaction mechanism in which UDP-GlcA would bind first, followed by $NAD^+$ binding, and oxidation of the 4″ hydroxyl. The resulting NADH would be released from the enzyme first, preventing the rereduction of the 4″ ketone. This strategy would allow the enzyme to generate the correct UDP-4-keto-pentose product instead of UDP-Xylose. While this model is compatible with the available structural evidence, it awaits corroboration by a full kinetic characterization of ArnA dehydrogenase.

### Substrate Binding in ArnA Dehydrogenase Compared to Other SDR Enzymes

ArnA dehydrogenase belongs to the short-chain dehydrogenase/reductase (SDR) family of enzymes that catalyze $NAD(P)^+$-dependent dehydrogenase reactions with various sugar nucleotides (Jornvall et al., 1995). The *E. coli* enzyme UDP-Galactose epimerase (GALE) has been extensively studied both structurally and mechanistically, and it is perhaps the best-characterized member of the SDR family (Thoden et al., 1996a, 1996b, 1996c, 1997a, 1997b, 2000, 2002; Thoden and Holden, 1998). Comparison of ArnA_DH with GALE allowed the modeling of UDP-GlcA and $NAD^+$ binding to ArnA (Gatzeva-Topalova et al., 2004). The current ligand bound structure confirms the location of the active site and provides a refined view of the substrate binding determinants.

Interestingly, the residues responsible for UDP-GlcA binding (Figure 5B) are well conserved not only in ArnA orthologs from other bacteria, but also in all UDP-Xylose synthases mentioned above (with the exception of $Y_{613}$, which is part of a four amino acid insertion in ArnA not present in the UDP-Xylose synthases) (see [Gatzeva-Topalova et al., 2004] and its supplemental data). However, those residues are not conserved in GALE in spite of binding a substrate similar to that of ArnA (GALE binds UDP-glucose/galactose instead of UDP-GlcA). This is likely due to the fact that SDR enzymes catalyzing epimerization reactions, like GALE and WbpP, need to flip the sugar ring about the bond linking the glycosidic oxygen and the β phosphate to accomplish epimerization (Ishiyama et al., 2004; Thoden et al., 2002). Therefore, it is advantageous for those enzymes to have a loose-fitting sugar binding pocket that can accommodate ring flipping (Ishiyama et al., 2004). Since no ring flipping is required for the oxidative decarboxylation reaction catalyzed by ArnA, more stringent binding of the glucuronate moiety is likely to constrain the substrate to a catalytically favorable conformation. In addition, mutating residue $R_{619}$ in ArnA to the corresponding residue in GALE (R619Y) not only completely abolished decarboxylation, but also failed to catalyze epimerization to UDP-Galacturonic acid (data not shown), further suggesting tighter binding of the sugar ring in ArnA compared to epimerases.

Many residues involved in $NAD^+$ binding by SDR enzymes are retained in ArnA dehydrogenase. However, the total number of contacts between the protein and the ADP moiety (the moiety common to $NAD^+$ and the ATP bound in the ligand bound structure) is smaller in ArnA than in GALE (8 in ArnA versus 17 in GALE). This is in agreement with

ArnA using $NAD^+$, which is bound, reduced, and released as NADH, as a true substrate, while GALE uses $NAD^+$ in a full reaction cycle (like UDP-Xylose synthase) as a coenzyme that remains tightly bound to the enzyme at all times (Ishiyama et al., 2004; Thoden et al., 1996a, 1996b, 1996c, 1997b).

## A Putative Catalytic Mechanism for ArnA Dehydrogenase

The reaction catalyzed by the ArnA dehydrogenase domain is a two-step process that includes: (i) the $NAD^+$-dependent oxidation of the UDP-GlcA $C_4''$ position, and (ii) decarboxylation of the β-ketoacid to yield UDP-4-keto-pentose (Figure 6).

The first step is similar to the oxidation step catalyzed by many SDR enzymes, including GALE, dTDP-D-Glucose 4,6-Dehydratase, and ADP-L-glycero-D-man-noheptose 6-epimerase, among others. The reaction mechanism has been extensively studied in these enzymes (Allard et al., 2001; Babbitt et al., 1995; Beis et al., 2003; Deacon et al., 2000; Thoden et al., 1997a, 2000; Vogan et al., 2004). In all cases, a serine/threonine-tyrosine-lysine catalytic triad was shown to be responsible for catalysis. In ArnA dehydrogenase, these three residues correspond to $T_{432}$, $Y_{463}$, and $K_{467}$ and are structurally conserved (Gatzeva-Topalova et al., 2004). Therefore, the first step in ArnA catalysis is likely to proceed by a similar mechanism. In this model, $Y_{463}$ acts as the general base catalyst abstracting a proton from the 4″-OH of UDP-glucuronate either directly or through a proton relay mechanism facilitated by $T_{432}$ (Gatzeva-Topalova et al., 2004; Thoden et al., 2000). In the ligand bound structure of ArnA, the $O^{\gamma}$ of $T_{432}$ is 2.5 Å away from the 4″-OH of the substrate, while the $O^{\eta}$ of $Y_{463}$ is almost 5 Å away. Therefore, a proton relay mechanism is very likely at play in ArnA. The third residue in the triad, $K_{467}$, would lower the *pKa* of $Y_{463}$ and enhance the reactivity of $NAD^+$ (Swanson and Frey, 1993) that accepts hydride transfer from the sugar C4″, yielding the UDP-4-keto-hexauronic acid intermediate (Figure 6).

The decarboxylation of the UDP-4-keto-hexauronic acid intermediate is the second step in the reaction that yields the final product, UDP-4-keto-pentose. The mutagenesis results presented here suggest a catalytic role for residues $R_{619}$ and $S_{433}$ in the decarboxylation step. While it is possible that the mutations affect the affinity of the enzyme for the UDP-GlcA, the following lines of evidence support a catalytic role for the residues: (i) the activity measurements were carried out at concentrations of substrates that are saturating for the wild-type enzyme ([UDP-GlcA] = 1 mM, more than 15-fold its apparent $K_m$ of 54 μM [Gatzeva-Topalova et al., 2004]); (ii) increasing the UDP-GlcA concentrations 5-fold had no effect on the activity of the S433A mutant and only a minor effect in the activity of the R619M mutant; (iii) the alternative $R_{619}$ mutants R619Y and R619E had undetectable activity even after overnight incubations; and (iv) these residues contribute only one ($S_{433}$) or two ($R_{619}$) hydrogen bonding interactions between ArnA and UDP-GlcA (Figure 5) out of a total of 15. We therefore consider it unlikely that $R_{619}$ and $S_{433}$ are only involved in substrate binding instead of catalysis.

We propose a mechanism for UDP-4-keto-hexa-uronic acid decarboxylation in which $R_{619}$ and $S_{433}$ play catalytic roles as depicted in Figure 7. In this model, both $S_{433}$ and $R_{619}$ initially hydrogen bond the carboxylate group of UDP-GlcA. The decarboxylation reaction proceeds via an enolate intermediate that would adopt a half chair conformation bringing the 4″ oxygen closer to $S_{433}$ and $R_{619}$. Ser433 and the positive charge of the protonated $R_{619}$ may help stabilize the developing negative charge in the 4″ oxygen, while the protonated $R_{619}$ functions as a general acid, donating a proton to the C5′ to yield the final product. The R619M mutant would not be able to serve as a general acid, and its residual activity may be due to much less efficient proton transfer from the bulk solvent or a nearby residue in the active site. Inspection of the active site shows that the side chain carboxylate of $E_{434}$ is 4.8

Å away from the C5′ of UDP-GlcA. However, this residue is unlikely to be protonated at neutral pH and would thus be unable to serve as a general acid. Saturation mutagenesis studies would be required to fully assess the precise role of each residue in the active site (Warren et al., 1996).

### Implications for Inhibitor Design

Both the dehydrogenation and transformylation reactions catalyzed by ArnA are required for lipid A modification with Ara4N and bacterial resistance to polymyxin (Breazeale et al., 2005; Roland et al., 1993, 1994; Shafer et al., 1984). This makes ArnA a good potential target for the design of new anti-infective compounds. Such inhibitors would make bacteria more susceptible to the antimicrobial activity of CAMPs and antibiotics of the polymyxin family. However, given the substrate similarities between ArnA_DH and human enzymes like UDP-Xylose synthase, the design of selective inhibitors may prove challenging. We propose that the substrate-induced conformational changes described here may provide a route to inhibitor selectivity. Since UDP-Xylose synthases use $NAD^+$ in a full reaction cycle, they are likely to have the $NAD^+$ coenzyme very tightly bound at all times, as observed for SDR enzymes that utilize $NAD^+$ in this manner. If the proposed ordered mechanism for ArnA is correct, UDP-GlcA analogs with extended groups at the 4″ position of the sugar may be able to bind preferentially to ArnA. They would occupy the UDP-GlcA site and part of the nicotinamide binding site that would be free in ArnA, but not in UDP-Xylose synthases. We await the synthesis of such analogs to test this intriguing hypothesis.

## Experimental Procedures

### Protein Purification

The ArnA full-length and ArnA dehydrogenase domains were expressed and purified as described previously (Gatzeva-Topalova et al., 2004). Point mutations in the ArnA dehydrogenase domain (R619M, R619Y, R619E, S433A, and S433T) were introduced by using the QuickChange site-directed mutagenesis kit (Stratagene) according to the manufacturer's instructions. During the mutagenesis procedure, a unique restriction site was also introduced (by silent mutation) next to the site of the point mutation to facilitate the selection of clones containing the mutant. After the introduction of the mutation, the vector was transformed into *E. coli* XL-10 cells (Stratagene) and plated on LB kanamycin plates. Plasmids were isolated by using the QIAprep Spin Miniprep kit (Qiagen). Clones carrying the mutation were identified by restriction digest taking advantage of the introduced unique restriction sites and were sequenced to ensure the absence of random mutations. The resulting mutants were overexpressed and purified as described for the wild-type ArnA dehydrogenase domain (Gatzeva-Topalova et al., 2004).

### Expression of Selenomethionine-Labeled ArnA Full-Length

The plasmid pETArnA (a generous gift from Prof. C. Raetz) was transformed into *E. coli* Rosetta (DE3) cells (Novagen). A 50 ml culture from a single colony containing 30 μg/ml kanamycin was grown overnight at 37°C. Two 10 ml aliquots were taken, spun down to remove LB media, and resuspended in 10 ml M9 minimal media supplemented with 30 μg/ml kanamycin. The resuspended bacterial pellets were used to start two 1 liter cultures in M9 minimal media containing 30 μg/ml kanamycin and were grown at 37°C to an $OD_{600}$ of ~0.6. At that point, the flasks were moved to room temperature, and methionine synthesis was inhibited by adding 100 mg/l D-lysine, D-phenylalanine, and D-threonine and 50 mg/l D-isoleucine and D-valine. In addition, 60 mg/l D/L selenomethionine (Se-Met, Sigma) was added. After 20 min, protein expression was induced with 0.4 mM isopropyl-1-β-D-thiogalactopyranoside (IPTG, Gold Bio Technology, Inc.) and grown for 6 hr at room temperature. Cells were harvested by centrifugation, and the protein was purified as

described for wild-type ArnA (Gatzeva-Topalova et al., 2004). The level of Se-Met incorporation was 88% as determined by amino acid analysis (AAA Service Laboratory, Inc.).

### ArnA Full-Length: Crystallization and Data Collection

ArnA full-length was preincubated for 30 min on ice with 3 mM UDP-GlcA and 3 mM $MgSO_4$ to give a final concentration of 6.0 mg/ml. Crystallization was attempted by the hanging drop method of vapor diffusion at 16°C (protein:precipitant ratio of 2.0 μl:2.0 μl). A condition consisting of 0.1 M MES (pH 7.0), 10% ethylene glycol, 9% polyethylene glycol 8000, 14 mM 2-mercaptoethanol, and 10 mM ATP yielded two different crystal forms with rhombohedral and orthorhombic morphologies. Initial diffraction analysis showed that the rhombohedral crystals belonged to space group R3 and typically diffracted to 3.5–4.0 Å resolution with slight anisotropy. Unit cell dimensions for these crystals were a = b = 150.9 Å, c = 218.4 Å, α = β = 90°, γ = 120° and contained two molecules per asymmetric unit (solvent content = 61.5%). The orthorhombic crystals belonged to $P2_12_12_1$ space group, with typical unit cell dimensions of a = 151.7, b = 166.2, c = 262.0, α = β = γ = 90° and six molecules per asymmetric unit (solvent content of 66.5%). These orthorhombic crystals diffracted to ~3.0 Å resolution at a synchrotron source. Crystallization of Se-Met-labeled protein was also attempted. We were only able to obtain the R3 crystal form with Se-Met-labeled protein after optimizing the crystallization conditions to 0.1 M MES (pH 6.75), 8% ethylene glycol, 9% polyethylene glycol 8000, 5 mM DTT, and 10 mM ATP. These crystals diffracted to the same resolution as the native crystals.

Prior to X-ray data collection, the Se-Met R3 crystals were transferred to a cryoprotecting solution composed of mother liquor containing 3 mM UDP-GlcA, 3 mM $MgSO_4$, and 15% w/v dextrose, soaked for 3 min, then transferred to the same cryoprotecting solution containing 30% w/v dextrose and flash cooled to 100°K in a nitrogen gas stream. $P2_12_12_1$ crystals were cryoprotected in mother liquor containing 3 mM UDP-GlcA, 3 mM $MgSO_4$, and 25% v/v glycerol, soaked for 1 hr, and flash cooled in a nitrogen stream. A 3.7 Å data set from the Se-Met-labeled R3 crystals and a 3.0 Å data set for the native $P2_12_12_1$ crystals were collected on beam line 8.2.2 at the Advanced Light Source at Lawrence Berkeley National Laboratory. Data were indexed and integrated with DENZO and scaled with SCALEPACK (Otwinowski and Minor, 1997). X-ray data collection statistics for both sets are shown in Table 1.

### ArnA Full-Length: Structure Determination and Refinement

The structure of ArnA was solved by molecular replacement by using the structures of the individual domains solved previously to 1.7 Å (ArnA transformylase domain, PDB ID: 1YRW [Gatzeva-Topalova et al., 2005]) and 2.4 Å (ArnA dehydrogenase domain, PDB ID: 1U9J [Gatzeva-Topalova et al., 2004]) as search models. Rotation/translation searches were performed with the program AMoRe (Navaza, 2001) and data between 15 and 4.5 Å using the R3 data set collected at the peak absorption wavelength of Se (λ = 0.9795). This data set was chosen despite the lower resolution because it contained only two protomers per asymmetric unit, compared to six in the case of the better diffracting $P2_12_12_1$ crystals. Rotation/translation searches allowed the location of two ArnA_DH molecules and one of the ArnA_TF molecules. Noncrystallographic symmetry (NCS) operation relating the two copies of ArnA_DH was computed and used to place the second copy of ArnA_TF in the asymmetric unit. Inspection of the crystal packing revealed no unfavorable molecular contacts. Prior to refinement with the program CNS (Brünger et al., 1998), 10% of the data were removed for crossvalidation. Several rounds of rigid body refinement followed by simulated annealing with torsion angle dynamics (Brünger et al., 1990, 1997) and domain B factor refinement dropped the $R_{work}$ from 47.8% to 35.0% and the $R_{free}$ from 48.6% to

41.7%. At this point, phases derived from the model were used to compute an anomalous difference Fourier map. Most methionines in both copies of the ArnA_DH and ArnA_TF domains coincided with anomalous difference peaks. Crystallographic symmetry operations applied to the model allowed the assembly of the biological hexamer, which was then used as a search model to solve the structure of the orthorhombic crystals by molecular replacement. Rotation/translation searches were again performed with the program AMoRe and data to 5 Å resolution, which yielded three equivalent solutions reflecting the 3-fold symmetry of the model. The same three solutions were obtained by using data in various resolution shells, and, in every case, they were well above the noise level. Prior to refinement with CNS, 10% of the data were removed for crossvalidation. The model was subjected to a round of rigid body refinement followed by domain B factor refinement with data to 4.0 Å. Model phases were improved by solvent flipping, as implemented in CNS (solvent content of 66%), and were used to compute an $F_0 \exp(\alpha_{calc})$ map. All models coincided generally well with the electron density, with the exception of one copy of the ArnA_TF domain, which appeared to be displaced from the density. A round of rigid body refinement with the MLHL target function (maximum likelihood with the solvent-flipped phase probability distribution) locked the stray ArnA_TF domains in the correct position. Tight (300 kcal $mol^{-1}$ $Å^{-2}$) noncrystallographic symmetry (NCS) restrains were set up with separate operators relating ArnA_DH and ArnA_TF domains. The model was then subjected to rounds of simulated annealing with torsion angle dynamics and group B factor refinements with data to 3.2 Å resolution. At this point, the R factor was 0.322 ($R_{free}$ = 34.5). Model phases were again improved by solvent flipping, and a new electron density map was calculated. Inspection of the map revealed a significant conformational change in residues 500–509 as well as clear density for residues 605–616, which were missing in our model. These regions were manually rebuilt with the program O (Jones, 1978). The model was subjected to several rounds of simulated annealing with Cartesian dynamics, followed by positional and B factor refinement with NCS restrains. Iterative rounds of manual rebuilding followed by positional and B factor refinement in which the NCS restrains were progressively relaxed were performed until no further improvement of the $R_{free}$ factor was observed ($R_{work}$ of 0.243 and $R_{free}$ of 0.261). At this point, electron density maps showed clear density for ATP and UDP-GlcA molecules in the dehydrogenase domain of each of the protomers, and they were added to the model. The final rounds of positional and atomic B factor refinement were carried out with NCS restrains relaxed to 40 kcal $mol^{-1}$ $Å^{-2}$ (ArnA_TF domain) and 80 kcal $mol^{-1}$ $Å^{-2}$ (ArnA_DH domain). The final model ($R_{work}$ of 0.225 and $R_{free}$ of 0.247) has good stereochemistry, as determined by using the program PROCHEK (Laskowski et al., 1993), with all amino acids lying in the most favorable or allowed regions on the Ramachandran plot. No electron density was observed for residues 35–42 in the transformylase domain or residues 305–313 in the interdomain linker (in chain D, the missing residues for the interdomain linker are 309–312). Refinement statistics and model stereochemistry are summarized in Table 1.

### ArnA Dehydrogenase Mutants: Structure Determination

Crystals of ArnA_DH mutants—R619M, R619Y, R619Mk and S433A—were obtained from conditions identical to those used for the wild-type ArnA_DH (Gatzeva-Topalova et al., 2004). Crystallization conditions were 2.0–2.1 M $(NH_4)_2SO_4$, 5 mM DTT, 100 mM MES (pH 6.75). For one of the mutants—S433T—we were not able to obtain crystals under these conditions. Like the wild-type ArnA_DH, all crystals belonged to space group $P4_132$, with dimensions similar to those of the wild-type protein (Table 1). Crystals were cryoprotected as previously described (Gatzeva-Topalova et al., 2004). Data were collected with a rotating anode generator by using $CuK_\alpha$ radiation and a Rigaku RAXIS $IV^{2+}$ detector, and on beam line 8.2.2 at the Advanced Light Source at Lawrence Berkeley National

Laboratory. Data were indexed and integrated with DENZO and scaled with SCALEPACK (Otwinowski and Minor, 1997). X-ray data collection statistics are shown in Table 1.

Prior to refinement with CNS, 10% of the data for each mutant was removed for crossvalidation. The model (ArnA_DH domain) was subjected to rigid body refinement followed by simulated annealing with Cartesian dynamics and several rounds of positional and B factor refinement. To reduce model bias, model phases were improved by solvent flipping. Inspection of the resulting map revealed no major difference between the wild-type and the mutant proteins. Refinement continued until no further improvement of the $R_{free}$ was observed. At this point, electron density maps showed clear density for several solvent molecules, sulfate ions (two in the S433A and R619M mutants, one in R619E and R619Y mutants), and glycerol molecules (R619M and S433A mutants), and these were added to the model. Iterative steps of positional and atomic B factor refinement followed by manual rebuilding were performed until no further improvement of R factors was achieved. Simulated annealing omit maps were calculated to validate the correctness of the structure in the area of the mutations. In all cases, the models had good stereochemistry, as determined by using the program PROCHEK (Laskowski et al., 1993), with all amino acids lying in the most favorable or allowed regions on the Ramachandran plot. Refinement statistics are shown in Table 1.

### Spectrophotometric Characterization of ArnA Dehydrogenase Mutants

The standard reaction mixture contained 25 mM Tris (pH 8.0), 5 mM 2-mercapto ethanol, 0.2 mg/ml BSA, 10% glycerol, 100 mM KCl, 3 mM $NAD^+$, and 1 mM (or 5 mM) UDP-glucuronic acid. The reaction was started with the addition of 200 nM wild-type and 1 μM mutant ArnA dehydrogenase. Enzyme activity was measured by following the increase of absorbance due to the produced NADH at 340 nm for 20 min. All enzyme assays were carried out at 37°C in a final volume of 800 μl.

## Acknowledgments

We are indebted to Gerry McDermott, Corie Ralston, J.J. Plecs, and the staff at the Advanced Light Source (ALS) for assistance in collecting crystallographic data. This work is based upon research carried out at the ALS, which is funded by the Department of Energy. This work was supported by a grant from the Cystic Fibrosis Foundation and a National Institutes of Heath (NIH) grant (AI060841-01) to M.C.S. Support for P.Z.G.-T. was provided by a NIH training grant (GM65103). Structural biology research at the University of Colorado at Boulder is supported in part by a grant from the William M. Keck Foundation.

## References

Allard ST, Giraud MF, Whitfield C, Graninger M, Messner P, Naismith JH. The crystal structure of dTDP-D-Glucose 4,6-dehydratase (RmlB) from *Salmonella enterica* serovar Typhimurium, the second enzyme in the dTDP-l-rhamnose pathway. J. Mol. Biol 2001;307:283–295. [PubMed: 11243820]

Babbitt PC, Mrachko GT, Hasson MS, Huisman GW, Kolter R, Ringe D, Petsko GA, Kenyon GL, Gerlt JA. A functionally diverse enzyme superfamily that abstracts the alpha protons of carboxylic acids. Science 1995;267:1159–1161. [PubMed: 7855594]

Baker SJ, Gunn JS, Morona R. The *Salmonella typhi* melittin resistance gene pqaB affects intracellular growth in PMA-differentiated U937 cells, polymyxin B resistance and lipopolysaccharide. Microbiol 1999;145:367–378.

Bar-Peled M, Griffith CL, Doering TL. Functional cloning and characterization of a UDP-glucuronic acid decarboxylase: the pathogenic fungus *Cryptococcus neoformans* elucidates UDP-xylose synthesis. Proc. Natl. Acad. Sci. USA 2001;98:12003–12008. [PubMed: 11593010]

Beis K, Allard ST, Hegeman AD, Murshudov G, Philp D, Naismith JH. The structure of NADH in the enzyme dTDP-d-glucose dehydratase (RmlB). J. Am. Chem. Soc 2003;125:11872–11878. [PubMed: 14505409]

Breazeale SD, Ribeiro AA, Raetz CR. Oxidative decarboxylation of UDP-glucuronic acid in extracts of polymyxin-resistant *Escherichia coli*. Origin of lipid a species modified with 4-amino-4-deoxy-L-arabinose. J. Biol. Chem 2002;277:2886–2896. [PubMed: 11706007]

Breazeale SD, Ribeiro AA, Raetz CR. Origin of lipid A species modified with 4-amino-4-deoxy-L-arabinose in polymyxin-resistant mutants of *Escherichia coli*. An aminotransferase (ArnB) that generates UDP-4-deoxyl-L-arabinose. J. Biol. Chem 2003;278:24731–24739. [PubMed: 12704196]

Breazeale SD, Ribeiro AA, McClerren AL, Raetz CRH. A formyltransferase required for polymyxin resistance in *Escherichia coli* and the modification of lipid A with 4-Amino-4-deoxy-L-arabinose. Identification and function of UDP-4-deoxy-4-formamido-L-arabinose. J. Biol. Chem 2005;280:14154–14167. [PubMed: 15695810]

Brünger AT, Krukowski A, Erickson J. Slow-cooling protocols for crystallographic refinement by simulated annealing. Acta Crystallogr. A 1990;46:585–593. [PubMed: 2206482]

Brünger AT, Adams PD, Rice LM. New applications of simulated annealing in X-ray crystallography and solution NMR. Structure 1997;5:325–336. [PubMed: 9083112]

Brünger AT, Adams PD, Clore GM, DeLano WL, Gros P, Grosse-Kunstleve RW, Jiang JS, Kuszewski J, Nilges M, Pannu NS, et al. Crystallography & NMR system: a new software suite for macromolecular structure determination. Acta Crystallogr. D Biol. Crystallogr 1998;54:905–921. [PubMed: 9757107]

Campbell RE, Mosimann SC, van De Rijn I, Tanner ME, Strynadka NC. The first structure of UDP-glucose dehydrogenase reveals the catalytic residues necessary for the two-fold oxidation. Biochemistry 2000;39:7012–7023. [PubMed: 10841783]

Deacon AM, Ni YS, Coleman WG Jr, Ealick SE. The crystal structure of ADP-L-glycero-D-mannoheptose 6-epimerase: catalysis with a twist. Struct. Fold. Des 2000;8:453–462.

Ernst RK, Yi EC, Guo L, Lim KB, Burns JL, Hackett M, Miller SI. Specific lipopolysaccharide found in cystic fibrosis airway *Pseudomonas aeruginosa*. Science 1999;286:1561–1565. [PubMed: 10567263]

Gatzeva-Topalova PZ, May AP, Sousa MC. Crystal structure of *Escherichia coli* ArnA (PmrI) decarboxylase domain. A key enzyme for lipid A modification with 4-amino-4-deoxy-L-arabinose and polymyxin resistance. Biochemistry 2004;43:13370–13379. [PubMed: 15491143]

Gatzeva-Topalova PZ, May AP, Sousa MC. Crystal structure and mechanism of *E. coli* ArnA (PmrI) transformylase domain. An enzyme for lipid A modification with 4-amino-4-deoxy-L-arabinose and polymyxin resistance. Biochemistry 2005;44:5328–5338. [PubMed: 15807526]

Ge X, Penney LC, van de Rijn I, Tanner ME. Active site residues and mechanism of UDP-glucose dehydrogenase. Eur. J. Biochem 2004;271:14–22. [PubMed: 14686915]

Gunn JS. Bacterial modification of LPS and resistance to antimicrobial peptides. J. Endotoxin Res 2001;7:57–62. [PubMed: 11521084]

Gunn JS, Miller SI. PhoP-PhoQ activates transcription of pmrAB, encoding a two-component regulatory system involved in *Salmonella typhimurium* antimicrobial peptide resistance. J. Bacteriol 1996;178:6857–6864. [PubMed: 8955307]

Gunn JS, Lim KB, Krueger J, Kim K, Guo L, Hackett M, Miller SI. PmrA-PmrB-regulated genes necessary for 4-aminoarabinose lipid A modification and polymyxin resistance. Mol. Microbiol 1998;27:1171–1182. [PubMed: 9570402]

Gunn JS, Ernst RK, McCoy AJ, Miller SI. Constitutive mutations of the *Salmonella enterica* serovar Typhimurium transcriptional virulence regulator phoP. Infect. Immun 2000a;68:3758–3762. [PubMed: 10816543]

Gunn JS, Ryan SS, Van Velkinburgh JC, Ernst RK, Miller SI. Genetic and functional analysis of a PmrA-PmrB-regulated locus necessary for lipopolysaccharide modification, antimicrobial peptide resistance, and oral virulence of *Salmonella enterica* serovar typhimurium. Infect. Immun 2000b; 68:6139–6146. [PubMed: 11035717]

Guo L, Lim KB, Gunn JS, Bainbridge B, Darveau RP, Hackett M, Miller SI. Regulation of lipid A modifications by *Salmonella typhimurium* virulence genes phoP-phoQ. Science 1997;276:250–253. [PubMed: 9092473]

Harper AD, Bar-Peled M. Biosynthesis of UDP-xylose. Cloning and characterization of a novel *Arabidopsis* gene family, UXS, encoding soluble and putative membrane-bound UDP-glucuronic acid decarboxylase isoforms. Plant Physiol 2002;130:2188–2198. [PubMed: 12481102]

Hoffmann JA, Kafatos FC, Janeway CA, Ezekowitz RA. Phylogenetic perspectives in innate immunity. Science 1999;284:1313–1318. [PubMed: 10334979]

Ishiyama N, Creuzenet C, Lam JS, Berghuis AM. Crystal structure of WbpP, a genuine UDP-N-acetylglucosamine 4-epimerase from *Pseudomonas aeruginosa*: substrate specificity in udp-hexose 4-epimerases. J. Biol. Chem 2004;279:22635–22642. [PubMed: 15016816]

Jones A. A graphics model building and refinement system for macromolecules. J. Appl. Crystallogr 1978;11:268–272.

Jornvall H, Persson B, Krook M, Atrian S, Gonzalez-Duarte R, Jeffery J, Ghosh D. Short-chain dehydrogenases/reductases (SDR). Biochemistry 1995;34:6003–6013. [PubMed: 7742302]

Laskowski RA, Macarthur MW, Moss DS, Thornton JM. Procheck: a program to check the stereochemical quality of protein structures. J. Appl. Crystallogr 1993;26:283–291.

Matsuzaki K. Why and how are peptide-lipid interactions utilized for self-defense? Magainins and tachyplesins as archetypes. Biochim. Biophys. Acta 1999;1462:1–10. [PubMed: 10590299]

Moriarity JL, Hurt KJ, Resnick AC, Storm PB, Laroy W, Schnaar RL, Snyder SH. UDP-glucuronate decarboxylase, a key enzyme in proteoglycan synthesis: cloning, characterization, and localization. J. Biol. Chem 2002;277:16968–16975. [PubMed: 11877387]

Navaza J. Implementation of molecular replacement in AMoRe. Acta Crystallogr. D Biol. Crystallogr 2001;57:1367–1372. [PubMed: 11567147]

Noland BW, Newman JM, Hendle J, Badger J, Christopher JA, Tresser J, Buchanan MD, Wright TA, Rutter ME, Sanderson WE, et al. Structural studies of *Salmonella typhimurium* ArnB (PmrH) aminotransferase: a 4-amino-4-deoxy-L-arabinose lipopolysaccharide-modifying enzyme. Structure 2002;10:1569–1580. [PubMed: 12429098]

Otwinowski Z, Minor W. Processing of X-ray diffraction data collected in oscillation mode. Methods Enzymol 1997;276:307–326.

Pattathil S, Harper AD, Bar-Peled M. Biosynthesis of UDP-xylose: characterization of membrane-bound AtUxs2. Planta. 2005 in press.

Perozich J, Leksana A, Hempel J. UDP-glucose dehydrogenase. Structural characteristics. Adv. Exp. Med. Biol 1995;372:79–84. [PubMed: 7484413]

Peschel A. How do bacteria resist human antimicrobial peptides? Trends Microbiol 2002;10:179–186. [PubMed: 11912025]

Roland KL, Martin LE, Esther CR, Spitznagel JK. Spontaneous pmrA mutants of Salmonella typhimurium LT2 define a new two-component regulatory system with a possible role in virulence. J. Bacteriol 1993;175:4154–4164. [PubMed: 8391535]

Roland KL, Esther CR, Spitznagel JK. Isolation and characterization of a gene, pmrD, from *Salmonella typhimurium* that confers resistance to polymyxin when expressed in multiple copies. J. Bacteriol 1994;176:3589–3597. [PubMed: 8206837]

Roman E, Roberts I, Lidholt K, Kusche-Gullberg M. Overexpression of UDP-glucose dehydrogenase in *Escherichia coli* results in decreased biosynthesis of K5 polysaccharide. Biochem. J 2003;374:767–772. [PubMed: 12775214]

Schiller JG, Lamy F, Frazier R, Feingold DS. UDP-glucose dehydrogenase from *Escherichia coli*. Purification and subunit structure. Biochim. Biophys. Acta 1976;453:418–425. [PubMed: 793622]

Scott MG, Hancock RE. Cationic antimicrobial peptides and their multifunctional role in the immune system. Crit. Rev. Immunol 2000;20:407–431. [PubMed: 11145218]

Shafer WM, Casey SG, Spitznagel JK. Lipid A and resistance of *Salmonella typhimurium* to antimicrobial granule proteins of human neutrophil granulocytes. Infect. Immun 1984;43:834–838. [PubMed: 6199303]

Shai Y. Mechanism of the binding, insertion and destabilization of phospholipid bilayer membranes by alpha-helical antimicrobial and cell non-selective membrane-lytic peptides. Biochim. Biophys. Acta 1999;1462:55–70. [PubMed: 10590302]

Swanson BA, Frey PA. Identification of lysine 153 as a functionally important residue in UDP-galactose 4-epimerase from *Escherichia coli*. Biochemistry 1993;32:13231–13236. [PubMed: 8241178]

Thoden JB, Holden HM. Dramatic differences in the binding of UDP-galactose and UDP-glucose to UDP-galactose 4-epimerase from *Escherichia coli*. Biochemistry 1998;37:11469–11477. [PubMed: 9708982]

Thoden JB, Frey PA, Holden HM. Crystal structures of the oxidized and reduced forms of UDP-galactose 4-epimerase isolated from *Escherichia coli*. Biochemistry 1996a;35:2557–2566. [PubMed: 8611559]

Thoden JB, Frey PA, Holden HM. High-resolution X-ray structure of UDP-galactose 4-epimerase complexed with UDP-phenol. Protein Sci 1996b;5:2149–2161. [PubMed: 8931134]

Thoden JB, Frey PA, Holden HM. Molecular structure of the NADH/UDP-glucose abortive complex of UDP-galactose 4-epimerase from *Escherichia coli*: implications for the catalytic mechanism. Biochemistry 1996c;35:5137–5144. [PubMed: 8611497]

Thoden JB, Gulick AM, Holden HM. Molecular structures of the S124A, S124T, and S124V site-directed mutants of UDP-galactose 4-epimerase from *Escherichia coli*. Biochemistry 1997a; 36:10685–10695. [PubMed: 9271499]

Thoden JB, Hegeman AD, Wesenberg G, Chapeau MC, Frey PA, Holden HM. Structural analysis of UDP-sugar binding to UDP-galactose 4-epimerase from *Escherichia coli*. Biochemistry 1997b; 36:6294–6304. [PubMed: 9174344]

Thoden JB, Wohlers TM, Fridovich-Keil JL, Holden HM. Crystallographic evidence for Tyr 157 functioning as the active site base in human UDP-galactose 4-epimerase. Biochemistry 2000;39:5691–5701. [PubMed: 10801319]

Thoden JB, Henderson JM, Fridovich-Keil JL, Holden HM. Structural analysis of the Y299C mutant of *Escherichia coli* UDP-galactose 4-epimerase. Teaching an old dog new tricks. J. Biol. Chem 2002;277:27528–27534. [PubMed: 12019271]

Vogan EM, Bellamacina C, He X, Liu HW, Ringe D, Petsko GA. Crystal structure at 1.8 Å resolution of CDP-D-glucose 4,6-dehydratase from *Yersinia pseudotuberculosis*. Biochemistry 2004;43:3057–3067. [PubMed: 15023057]

Warren MS, Marolewski AE, Benkovic SJ. A rapid screen of active site mutants in glycinamide ribonucleotide transformylase. Biochemistry 1996;35:8855–8862. [PubMed: 8688421]

Yang L, Weiss TM, Lehrer RI, Huang HW. Crystallization of antimicrobial pores in membranes: magainin and protegrin. Biophys. J 2000;79:2002–2009. [PubMed: 11023904]

Zasloff M. Antimicrobial peptides of multicellular organisms. Nature 2002;415:389–395. [PubMed: 11807545]

Zhou Z, Lin S, Cotter RJ, Raetz CR. Lipid A modifications characteristic of *Salmonella typhimurium* are induced by NH4VO3 in *Escherichia coli* K12. Detection of 4-amino-4-deoxy-L-arabinose, phosphoethanolamine and palmitate. J. Biol. Chem 1999;274:18503–18514. [PubMed: 10373459]

**Figure 1. Proposed Biosynthetic Pathway for the Addition of 4-Amino-Arabinose to Lipid A**

This figure has been adapted from Breazeale et al., 2005. The pathway starts with UDP-Glucose being oxidized by UDP-Glucose dehydrogenase (Ugd) to form UDP-Glucuronic acid (UDP-GlcA). ArnA, the first pathway-specific enzyme, catalyzes the $NAD^+$-dependent oxidation of UDP-GlcA to UDP-4-keto-pentose with its C-terminal domain. The next enzyme in the pathway, ArnB, catalyzes the transamination reaction, leading to the formation of UDP-β-(4-deoxy-4-amino-L-arabinose) (UDP-Ara4N). This product is then transiently formylated by the N-terminal domain of ArnA to produce UDP-β-(4-deoxy-4-formamido-L-arabinose) (UDP-Ara4-Formyl-N). The formylated species is transferred to a membrane bound undecaprenyl phosphate by ArnC. Additional enzymes in the pathway, which have not yet been fully characterized, complete the pathway, deformylating undecaprenyl-Ara4-FN and transferring Ara4N to lipid A.

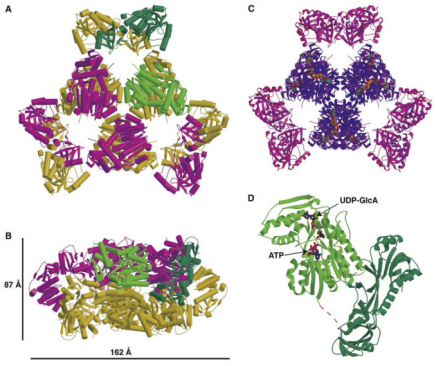


**Figure 2. Structure of ArnA**

ArnA forms a dimer of trimers and adopts the shape of a three-blade propeller.

(A) Ribbon diagram of the ArnA hexamer (top view). The helixes are shown as cylinders. The bottom trimer is colored in gold, and the top trimer is colored in magenta. One of the monomers is colored differently, such that the ArnA N-terminal transformylase domain is colored in dark green and the C-terminal dehydrogenase domain is colored in light green.

(B) Side view of the ArnA hexamer (coloring scheme as in [A]).

(C) Top view of the ArnA hexamer colored by temperature factor from purple (lowest) to red (highest). The ligands UDP-GlcA and ATP are shown as space-filling models (nitrogen is colored in green, oxygen in red, carbon in gray, and phosphorus in yellow).

(D) Cartoon representation of a single ArnA protomer. The ArnA transformylase domain is colored in dark green, and the ArnA dehydrogenase domain is colored in light green. The ligands are presented as stick models. UDP-GlcA binds in the C-terminal subdomain of ArnA dehydrogenase, and the $NAD^+$ analog, ATP, binds in the N-terminal (Rossmann fold) subdomain.

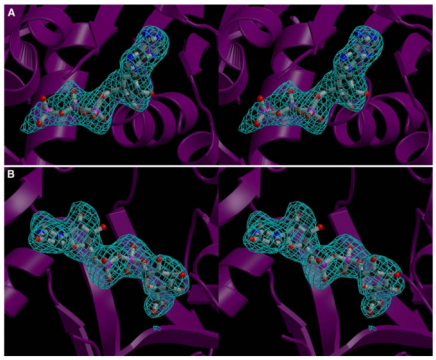


**Figure 3. Stereo View of Representative Electron Density for the Two Ligands**

The maps are $F_o - F_c$ simulated annealing omit maps, computed with phases calculated from models in which the ligands were omitted.

(A) Electron density in the ATP binding site contoured at 5σ. The protein is shown as a ribbon diagram colored in magenta, and the refined substrate model is superimposed on the density for reference.

(B) Electron density for the UDP-GlcA binding site contoured at 5σ, colored as in (A).

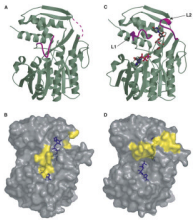

**Figure 4. Conformational Changes in ArnA_DH**

(A) Structure of the ligand-free ArnA dehydrogenase domain (PDB_ID: 1U9J). The 500–509 loop that blocks the $NAD^+$ binding site is colored in magenta. The disordered loop, loop 605–616, is shown as a dotted line colored in magenta.

(B) Structure of the ATP/UDP-GlcA ligand bound ArnA_DH domain. The 500–509 loop (L1) is displaced 17 Å (measured at the Cα of the central residue I506) compared to the ligand-free structure, opening the $NAD^+$ binding site. The 605–616 loop becomes ordered into a one-turn helix, followed by a loop that lines the UDP-GlcA binding site (L2).

(C) Transparent surface model of the ligand-free ArnA dehydrogenase domain. For reference, the positions of the two ligands from the ligand bound structure are shown as blue sticks. The 500–509 loop is colored in yellow, blocking the $NAD^+$ binding site, while the UDP-GlcA binding site appears open. Residues 604 and 617, which represent the ends of the disordered 605–616 loop, are also colored yellow.

(D) Transparent surface model of the ATP/UDP-GlcA bound structure. Both ligands are presented as blue sticks. A large conformational change in the 500–509 region, as well as stabilization of the 605–616 region, opens the $NAD^+$ binding site but effectively traps UDP-GlcA in its active site.

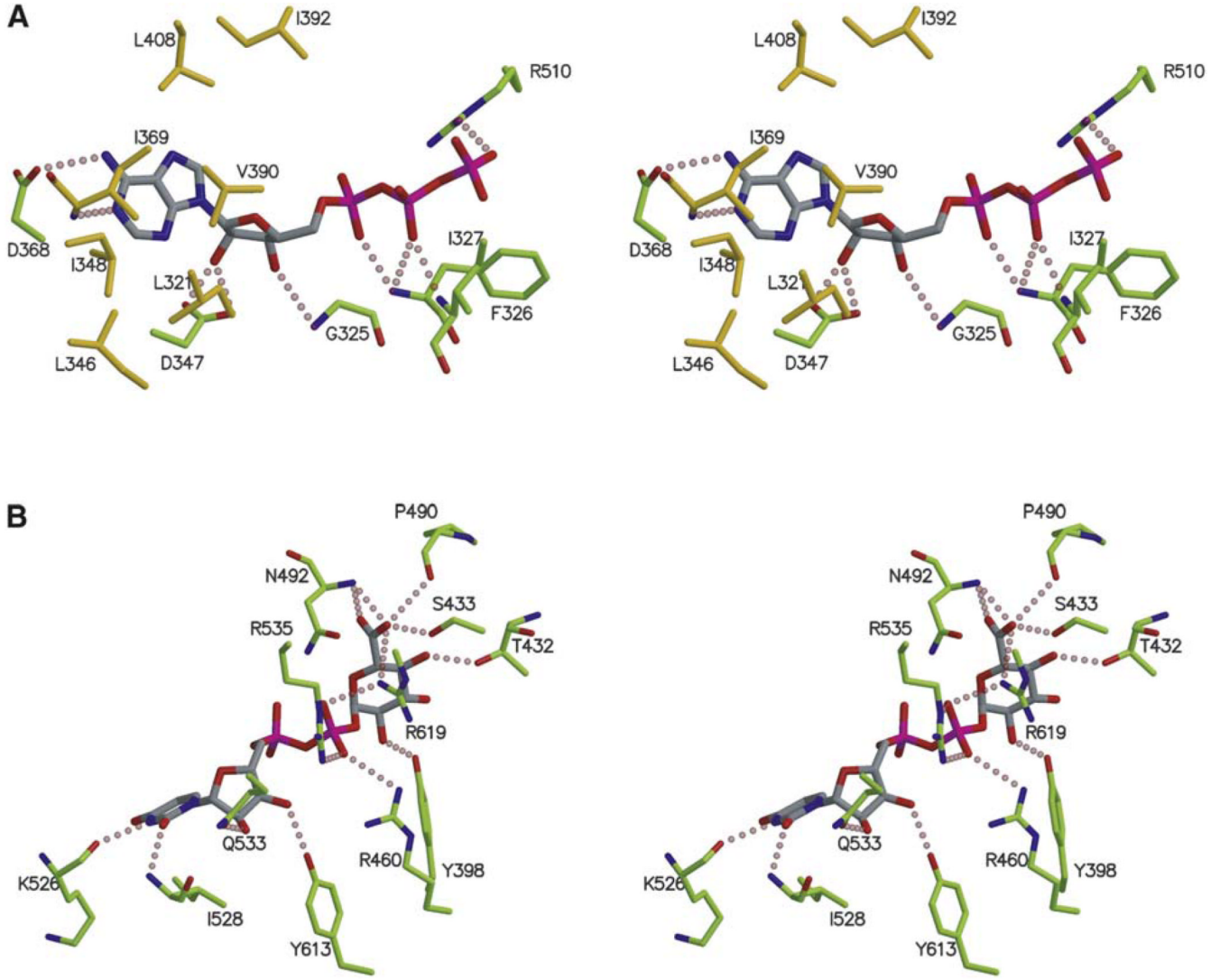


**Figure 5. Substrate Binding Sites in the ArnA_DH**

(A) The ATP binding site. The adenosine ring lies in a hydrophobic pocket formed by residues $I_{321}$, $L_{346}$, $I_{348}$, $I_{369}$, $V_{390}$, $I_{392}$, and $L_{408}$ (colored in yellow). Residues of the protein that contribute hydrogen bonding interactions are colored in green.

(B) The UDP-GlcA binding site. Protein residues forming hydrogen bonds with the substrate are colored in green.

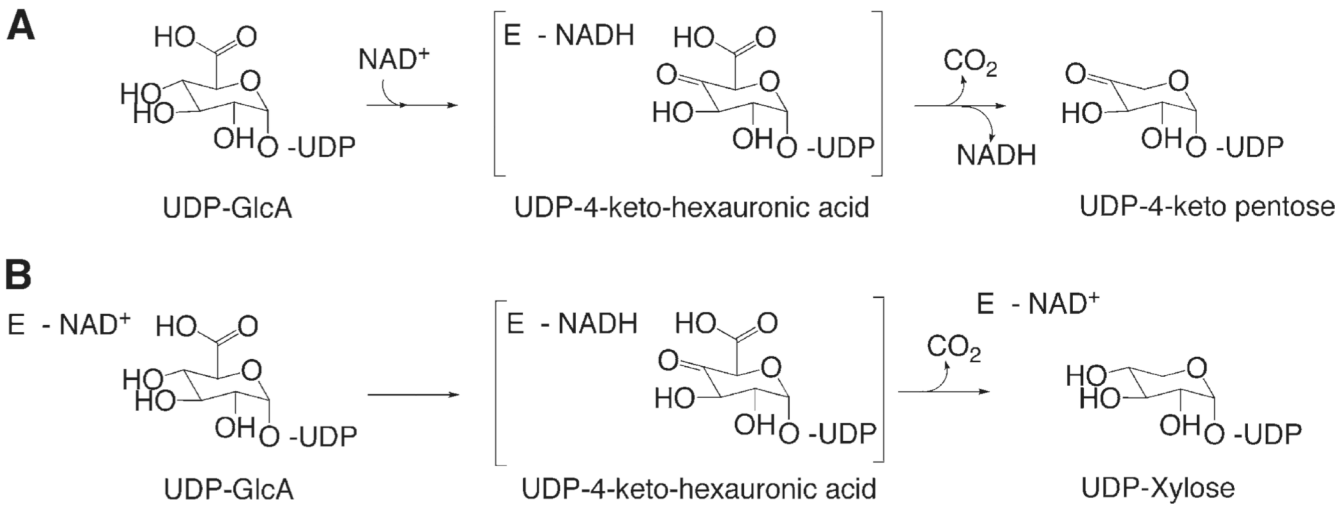


**Figure 6. Enzymes Catalyzing the Oxidative Decarboxylation of UDP-GlcA**

(A) ArnA dehydrogenase domain. In this enzyme, $NAD^+$ is used to oxidize UDP-GlcA to UDP-4-keto-hexauronic acid with the release of NADH.

(B) UDP-Xylose synthases. These enzymes use $NAD^+$ as a cofactor. It is utilized to oxidize the 4″ hydroxyl of UDP-GlcA just as in ArnA_DH. However, the decarboxylated 4-keto-pentose is rereduced by NADH to generate UDP-Xylose without net consumption of $NAD^+$.

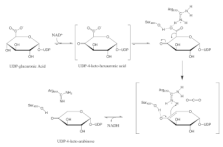

**Figure 7. Proposed Mechanism for the UDP-4-Keto-Hexauronic Acid Decarboxylation**

The substrate, UDP-GlcA, is first oxidized at the glucosyl $C_4''$ by $NAD^+$ to generate UDP-4-keto-hexauronic acid. Residues $S_{433}$ and $R_{619}$ initially hydrogen bond to the carboxyl group of UDP-GlcA. The formation of carbon dioxide is accompanied by the formation of an enolate intermediate that would adopt a half chair conformation, bringing the 4″ oxygen closer to $S_{433}$ and $R_{619}$. The developing negative charge may be stabilized by the positive change of $R_{619}$ and hydrogen bonding to $S_{433}$. The residue $R_{619}$ may function as a general acid, donating a proton to the $C_5''$ to yield the final product, UDP-4-keto pentose.

**Table 1**

Data Collection and Refinement Statistics

| | R3 ArnA | $P2_12_12_1$ ArnA | R619M | R619Y | R619E | S433A |
|---|---|---|---|---|---|---|
| Data Collection Statistics | | | | | | |
| Wavelength (Å) | 0. 9795 | 1.1808 | 1.54 | 1.54 | 1.0781 | 1.54 |
| Space group | R3 | $P2_12_12_1$ | $P4_132$ | $P4_132$ | $P4_132$ | $P4_132$ |
| Cell parameters (Å) | a = b = 150.9, c = 218.4 | a = 151.7, b = 166.2, c = 262.0 | a = b = c = 150.4 | a = b = c = 150.2 | a = b = c = 150.3 | a = b = c = 150.4 |
| Resolution (Å) | 30.0−3.70 | 50.0−3.0 | 30.0−2.4 | 30.0−2.7 | 30.0−2.3 | 30.0−2.5 |
| Highest resolution shell (Å) | 3.83−3.70 | 3.11−3.0 | 2.49−2.4 | 2.8−2.7 | 2.38−2.3 | 2.59−2.5 |
| Measured reflections | 59,540 (5,914) | 166,227 (47,647) | 175,106 (16,021) | 102,693 (9,445) | 180,121 (17,703) | 223,475 (21,760) |
| Unique reflections | 18,668 (1,908) | 132,644 (13,215) | 23,212 (2,262) | 16,479 (1,615) | 26,139 (2,564) | 20,730 (2,010) |
| I/σ | 13.1 (2.4) | 14.8 (3.9) | 20.7 (4.5) | 22.2 (4.6) | 21.7 (5.0) | 23.2 (4.4) |
| Redundancy | 3.2 (3.1) | 1.3 (3.6) | 7.5 (7.1) | 6.2 (5.8) | 6.9 (6.9) | 10.8 (10.8) |
| Data completeness (%) | 94.5 (97.0) | 99.2 (99.8) | 99.8 (99.2) | 98.8 (100.0) | 99.8 (100.0) | 100.0 (100.0) |
| $R_{merge}$ (%) | 8.4 (42.3) | 7.9 (34.9) | 8.6 (43.7) | 8.0 (41.0) | 9.4 (51.0) | 9.7 (57.8) |
| Refinement Statistics | | | | | | |
| $R_{work}$ | | 0.225 (0.317) | 0.203 (0.242) | 0.212 (0.274) | 0.200 (0.242) | 0.205 (0.258) |
| $R_{free}$ | | 0.247 (0.334) | 0.231 (0.311) | 0.260 (0.306) | 0.224 (0.253) | 0.246 (0.314) |
| Rmsd from ideal values | | | | | | |
| Bond lengths (Å) | | 0.008 | 0.01 | 0.01 | 0.01 | 0.008 |
| Bond angles (°) | | 1.42 | 1.47 | 1.49 | 1.45 | 1.37 |
| Mean B value ($Å^2$) | | 44.7 | 37.0 | 44.5 | 37.2 | 41.4 |
| B factor deviation bonds ($Å^2$) | | 0.97 | 1.27 | 1.41 | 1.22 | 1.22 |
| B factor deviation angles ($Å^2$) | | 1.69 | 2.02 | 2.30 | 1.93 | 2.00 |
| Ramachandran | | | | | | |
| Residues in favored region (%) | | 86.1 | 88.1 | 88.4 | 88.7 | 89.3 |
| Residues in allowed regions (%) | | 13.9 | 11.9 | 11.6 | 11.3 | 10.7 |

$R_{work} = \Sigma|F_{obs} - F_{calc}|/\Sigma F_{obs}$, where $F_{obs}$ = observed structure factor amplitude, and $F_{calc}$ = structure factor calculated from the model. $R_{free}$ is computed in the same manner as $R_{work}$, by using the test set of reflections. Values for the highest resolution bin are shown in parentheses.

**Table 2**

Activity of ArnA Dehydrogenase Mutants

| Enzyme | Rate, $nmol_{NADH} \cdot mg_{Ez}^{-1} \cdot min^{-1}$ | Fold Decrease in Activity |
|---|---|---|
| Wild-type ArnA _DH | 215.9 ± 0.4 | – |
| S433A (1 mM UDP-GlcA) | 6.33 ± 0.03 | 30 |
| S433A (5 mM UDP-GlcA) | 6.43 ± 0.10 | 30 |
| R619M (1 mM UDP-GlcA) | 0.26 ± 0.05 | 800 |
| R619M (5 mM UDP-GlcA) | 0.51 ± 0.10 | 400 |
| R619Y (1 mM UDP-GlcA) | 0.02 ± 0.02 | >10000 |
| S433T (1 mM UDP-GlcA) | 0.01 ± 0.02 | >10000 |
| R619E (1 mM UDP-GlcA) | 0.00 ± 0.02 | >10000 |

The activity of the mutants was measured spectrophotometrically by detecting the increase of absorbance at 340 nm due to the release of NADH. The substrates UDP-GlcA and $NAD^+$ were used at saturating concentrations (UDP-GlcA, 1 or 5 mM; NAD, 3 mM) for the wild-type enzyme ($K_m$, app [NAD] = 0.57 ± 0.09 mM; $K_m$, app [UDP-GlcA] = 0.054 ± 0.003 mM [Gatzeva-Topalova et al., 2004]).